Reprinted from Nature, Vol. 302, No. 5910, pp. 676-681, 21 April 1983

Three-dimensional architecture of a polytene nucleus

David A. Agard & John W. Sedat

Department of Biochemistry and Biophysics, University of California, San Francisco, California 94143, USA

The three-dimensional chromosome topography in an intact nucleus has been determined using fluorescently stained Drosophila *polytene chromosomes, optical fluorescence microscopy and newly developed, generally applicable, cellular image reconstruction techniques. The folding pattern is a complex mixture of parallel chromosomal segments and intertwined coils and shows extensive interaction of the chromosomes with the nuclear envelope.*

ALTHOUGH much has been learned about the structure of chromatin at the levels of greatest resolution[1-8], surprisingly little is known of its higher-order organization. Several investigators have examined the highest levels of chromatin organization in mitotic chromosomes, and both radial-loop[9] and sequential-coiling[10,11] models have been suggested (for review see ref. 12). Inoué[13], and our own work[14,15], suggest that in native preparations of insect sperm heads the highest level of DNA organization is a double-helical arrangement of an approximately 100-nm diameter fibre. The arrangement of chromosomes within the cell nucleus is even less well understood than the structure of the chromosomes themselves. This is primarily due to the previous lack of general methods for *in situ* analysis without disrupting the existing organization.

The notion that chromosomes are not randomly distributed within the nucleus goes back to the early 1900s, when Boveri postulated that the reproducible positioning of unique visual markers (for example, nuclear lobes in *Ascaris megacephala*) was due to a determined nuclear arrangement[16]. Although this idea fell into disfavour for a period, sufficient evidence has accumulated recently to help reestablish it. A nonrandom distribution of chromosomes on the metaphase plate has been reported in many species from plants[17] to man [18] (for review see ref. 19). Several authors have reported the specific end-to-end attachment or association of telomeres during prophase (see, for example, refs 20, 21), as well as a spatial polarization—centromeres and telomeres at opposite poles of the nucleus. The centromeres are generally grouped together during prophase and the degree of association appears to be under direct genetic control[22].

The chromosomal arrangements seen during prophase and metaphase have been postulated to be the remnants of (and consequently an argument for) chromosomal order in interphase. Indirect evidence from a variety of different experiments supports this hypothesis. Interphase chromosomes are attached to the nuclear envelope via specific chromosomal segments (centromeres, telomeres, and possibly other regions[23-26]). There is also some recent evidence that transcriptionally active genes are closely associated with the nuclear membrane[27]. More directly, analysis of the nonrandom distribution of radiation and mutagen induced chromosomal exchanges in somatic plant cells indicates that both homologous and nonhomologous chromosomes are nonrandomly arranged in interphase, and that this arrangement is not inconsistent with that observed during metaphase[28,29]. All of this evidence (much of it circumstantial) points to the existence of an ordered interphase arrangement of chromosomes.

That chromosome organization is important for gene expression is suggested by genetic studies. Perhaps the best example is the interaction of the *zeste* and *white* loci in *Drosophila*. Jack and Judd (ref. 30, see also ref. 31) reported that the *zeste* locus functions as a repressor of the *white* locus, and that repression only occurs if the two *white* alleles are physically adjacent or paired. The strength of repression was found to diminish with increasing separation. This suggests that there may be a close and defined association between loci on separate chromosomes, and that communication of regulatory signals may be spatially restricted.

In an attempt to understand the complex interactions between structure and function taking place at the chromosomal level, we have embarked on the direct determination of the spatial arrangement of *Drosophila melanogaster* chromosomes at different points in the cell cycle, and from nuclei in different developmental and transcriptional states. We report here a determination of the three-dimensional topography of chromosomes in an intact interphase nucleus. For these studies we chose polytene nuclei from *D. melanogaster* salivary glands, which are composed of cells in a well defined developmental

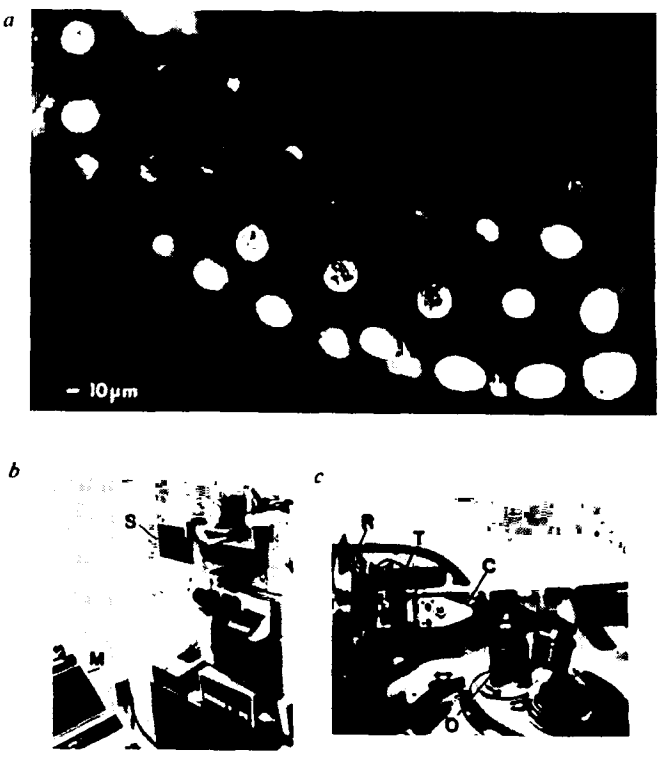

Fig. 1 *a*, An intact salivary gland from a third-instar *Drosophila* larva is shown stained for DNA with Hoechst 33258. The brightly fluorescing nuclei are clearly visible. *b*, The Zeiss Axiomat used for data collection under microprocessor control. The stepping motor connected to the focus control through an electromagnetic clutch is shown by the arrow (S), and is driven by the microprocessor (M). *c*, The tilting stage (C), has a rotation bearing (R) and translation motors (T) to align the sample mounted in a quartz capillary. The objective lens is also shown (O).

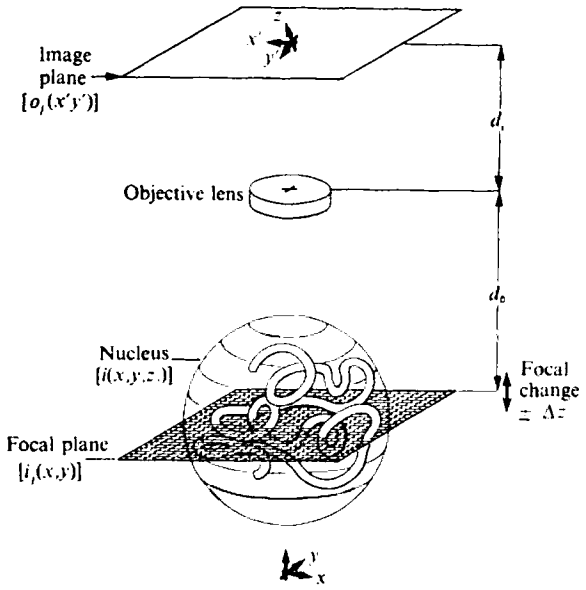

Fig. 2 A schematic representation of the optical sectioning method. The image distance d_i and the focal length of the lens f are fixed; the object distance, $d_o = fd_i/(d_i - f) = d_i/M$ (M = magnification). The image o_j is a composite of in-focus information from the focal plane i_j, and out-of-focus detail from the remainder of the specimen $i(x, y, z)$. The method described in the text allows the set of i_j (the sampled approximation of $i(x, y, z)$) to be determined from the set of observed images, the o_j.

state and so allow a structural comparison of functionally equivalent nuclei. Each of the polytene chromosomes is composed of ~1,024 haploid copies of the genome, interphase-arrested and arranged so that the genetic loci along the length of the chromosome are all in register[32]. This precise alignment gives rise to characteristic banding patterns that serve as markers for defined genetic loci. These greatly enlarged polytene chromosomes (3–4 μm diameter) are readily visualized by optical methods.

The topographical analysis reported here was made possible by a combination of DNA-specific fluorescent staining, optical microscopy and digital reconstruction together with enhancement techniques. This approach, essentially tomography at the cellular level, allows the structure and organization of entire cells, organelles, or their subfractions to be reconstructed in three-dimensions in essentially *in vivo* conditions. The use of optical sectioning (essentially a through-focal series) instead of physical sectioning allows a non-destructive analysis while retaining three-dimensional information. Fluorescence microscopy, using specific dyes or labelled monoclonal antibodies, allows the selective imaging of specific components in complex heterogeneous assemblies. A constrained deconvolution algorithm has been used to effectively eliminate the gaussian-emitter 'glow' effect characteristic of fluorescent imaging, resulting in a sharper, more detailed image.

Visualization of polytene chromosomes

Salivary glands from third instar *D. melanogaster* larvae were carefully removed by hand dissection and stained with the DNA-specific, non-intercalative fluorescent dye Hoechst H33258 as described elsewhere[10]. This dye only fluoresces when bound, and only binds to DNA. Thus only the DNA-containing structures are imaged, largely without interference from any proteinaceous or membranous structures within the cell. A non-intercalative dye was chosen to avoid chromosomal perturbations resulting from DNA-unwinding induced by intercalating dyes. Conditions were such as to minimize any artefacts arising from sequence-specific staining.

At the third instar developmental stage, the salivary glands are each composed of 140 giant cells (~70 μm diameter), arranged in a layer two cells thick. The fluoresent staining allows the polytene chromosomes within each 30–40 μm diameter nucleus to be visualized (Fig. 1). Owing to the complexity of the packing, only small segments of the individual polytene chromosomes can actually be seen in Fig. 1. Their slightly

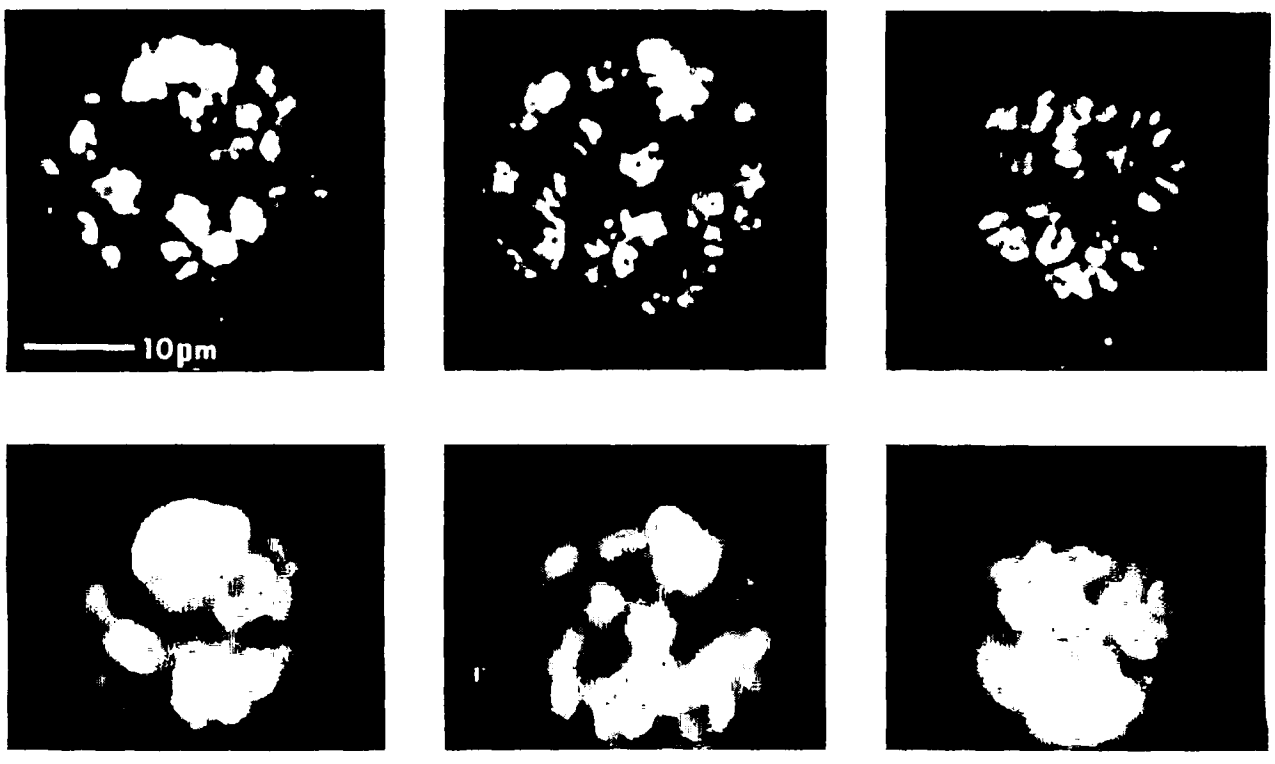

Fig. 3 Comparisons of images before (bottom) and after data processing (top) for three non-contiguous sections from the stack of 30 planes used. The data have been processed both to remove out-of-focus contamination and to remove the 'flare' due to fluoresence imaging. The major effect of the processing is to increase dramatically the definition between planes in the stack.

mottled appearance is the result of the barely resolved banding characteristic of polytene chromosomes. The banding pattern visualized with the Hoechst dye from fluorescent micrographs (not shown) is identical to that observed using standard squash staining procedures, which in future studies will be important for localizing specific genetic regions in the three-dimensional structure.

Three-dimensional data collection from thick specimens

Understanding the ways in which the individual chromosomes interact requires elucidation of the complex path followed by each chromosome through the nucleus. Mapping of this folding pattern by conventional microscopic techniques is very difficult owing to the conflicting requirements for high spatial resolution and very large depth of field. In those cases where the thickness of the object is comparable to the depth of focus, or where there is little information lost by defocus (as in electron microscopy), the object can be reconstructed from a set of tilted projections. We have used this method in the investigation of the non-crystalline three-dimensional arrangement of DNA in *Drosophila* sperm heads, which are only 0.4 μm in diameter[13,14].

For thicker specimens, it is necessary to reconstruct the object from a series of either physical or optical sections. Fragile structures are readily damaged by physical sectioning; and variations in section thickness, amount of shrinkage, and alignment errors can all introduce distortions into the reconstruction. By contrast, optical sectioning provides a non-destructive means of collecting three-dimensional data from thick samples and, uniquely, allows the analysis of living tissues. Nomarski optical sectioning methods have proved to be extraordinarily useful for biological studies; however, the cumulative build-up of scattering mass limits the useful specimen thickness to 15–20 μm. More seriously, such phase interference techniques provide a rather low-contrast view of the entire cellular contents. It is impossible to highlight specific macromolecular or chemically defined components.

The optical sectioning method we describe here combines the biological specificity and high contrast of fluorescence microscopy with the high resolution typical of Nomarski optics, and allows specimens with thickness considerably greater than 100 μm to be readily imaged. This approach is shown schematically in Fig. 2. The thick specimen is examined using a very high resolution, narrow depth-of-focus objective lens. In these conditions only a thin plane within the sample is visualized in-focus. The recorded image represents the summation of in-focus information from that plane with out-of-focus information from the remainder of the sample, the degree of defocus varying with the distance from the in-focus plane. From a complete set of images taken at different focal points, it is possible to remove computationally from each plane the contributions of all the other planes (see below).

The accuracy of the solution depends on both the quality of the data and the accuracy with which the contrast transfer function at each level of defocus can be determined. This requires a knowledge of the microscope's optical system, as well as a precise control of the exact amount of focal shift used to record each image. This was accomplished by modifying a Zeiss Axiomat microscope so that the focus could be driven by a 1,000 step per turn stepping motor providing a change in focus of 100 nm per step. In addition, the sample (mounted in a quartz capillary on a eucentric goniometer) can be rotated to provide tilted views of the same specimen as shown in Fig. 1*c*. The motors, the shutter and the film advance mechanism are all controlled by microcomputer (Fig. 1*b*).

Three-dimensional reconstruction of a whole nucleus

To reconstruct the polytene nucleus, a series of 30 photographic images, corresponding to planes separated by 1.2 μm, was digitized on a 120-μm raster (370 nm at the sample plane) to provide a set of 30 128×128 pixel images. Because each negative was scanned independently, it was necessary to align each image precisely with respect to the others. The most accurate and stable procedure found was systematically to vary the translations along the X and Y coordinates, the rotation angle, and the scale factor while searching for a minimum in the normalized error function:

$$R = \frac{\sum |I - I'|}{\sum |I|}$$

where I is the reference image and I' corresponds to the scaled, rotated, translated image intensity of the image being aligned, as obtained by quadratic interpolation[14]. The summations are carried out only over those points where I is above some threshold (to minimize the effects of background noise on the alignment). The resultant alignment is precise to approximately 0.2 pixels, with typical R values of from 3 to 8%.

The procedure for removing the out-of-focus information from each image plane was inspired by Castleman[33], but modified so that most operations were performed in Fourier transform space, thereby greatly speeding the calculations. This approach is more exact than that used by Weinstein and Castleman[34] to study stained neurones; theirs is an approximate method suitable primarily for very coarse sections (≥5 μm thick).

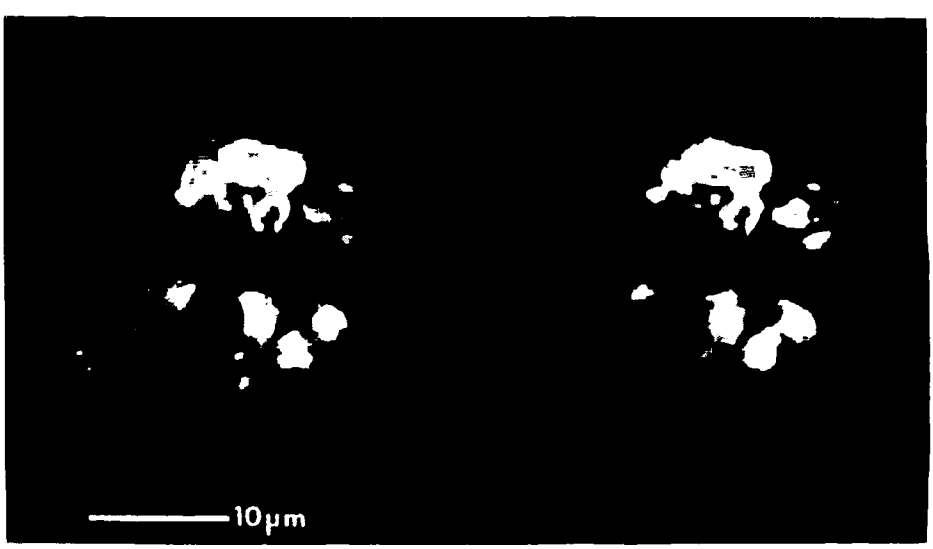

Fig. 4 A stereo perspective view of one hemisphere of the reconstructed three-dimensional 'DNA-density' map. The view is taken from the hollow central cavity (nucleolus) looking out.

The observed image o_j for any plane j is a composite of the 'true' density distribution i_j for that plane with the blurred contributions from the m planes above and the m' planes below

$$o_j = i_j + \sum_{\substack{k=j-m' \\ k \neq j}}^{j+m} i_k * s[\Delta z \cdot (k-j)] \quad (1)$$

where * represents the two-dimensional convolution operation, o_j and i_j are two-dimensional functions of the planar coordinates (x, y), s is the defocus blurring function, and Δz is the separation between planes. The modulation transfer function s is a radially symmetric function that varies with the amount of defocus $[\Delta z \cdot (j-k)]$ and the optical parameters of the microscope. Equation (1) can be recast by taking the Fourier transform of both sides of the equation, thus converting the convolution into a multiplication

$$O_j = I_j + \sum_{\substack{k=j-m' \\ k \neq j}}^{j+m} I_k \cdot S[\Delta z \cdot (k-j)] \quad (2)$$

where O, I, and S, respectively, are the Fourier transforms of o, i, and s. Given some initial guess ($n = 0$) for the Is (I^0), it is possible to generate an improved guess ($n+1=1$) (I^1) as follows

$$I_j^{n+1} = O_j - \sum_{\substack{k=j-m' \\ k \neq j}}^{j+m} I_k^n \cdot S[\Delta z \cdot (k-j)] \quad (3)$$

Thus, in an iterative fashion it is possible to develop a self-consistent solution to the three-dimensional convolution implied by equation (1). *Values for the deblurred images* (i_j) are determined by inverse Fourier transformation of the final I_j. The result is the determination of a set of images i_j, that when appropriately blurred and summed will equal, with arbitrary precision, the observed images o_j.

In practice the initial guess (I^0) is set equal to the observed (O). The number of sections that need be considered simultaneously ($m+m'$) depends on the choice of objective lens and the spacing between sections. With the ×63 (1.25 NA) oil lens used and with $\Delta z = 1.2$ μm, it was only necessary to consider simultaneously a stack of seven planes (three above and three below; $m = m' = 3$). Values for the optical contrast transfer function (S) for differing amounts of defocus were calculated according to the theory developed by Stokseth[35] using lens parameters obtained from Zeiss. In these computations the wavelength spread of the emitted light was neglected. For a higher-resolution analysis this could be included by appropriately modifying the contrast transfer function. The procedure converged to a solution after five iterations. Finally, the resultant in-focus three-dimensional image was enhanced using an iterative, constrained deconvolution technique described elsewhere[14,36]. Such post-processing is necessary to remove the 'glow' effect characteristic of fluorescent emitters due to light scatter, and provides an apparent resolution increase of two or three-fold, without significantly increasing the noise level. The ultimate obtainable effective in-plane resolution is about 100–200 nm but was limited here to about 500 nm by the coarse scanning interval used.

The result is an enhanced, three-dimensional 'DNA-density' map, which reveals the path through the nucleus followed by the DNA components within the polytene chromosomes. Before and after images of several individual sections are shown in Fig. 3 for comparison. A stereo representation of a hemisphere of the three-dimensional map viewed from the inside is shown in Fig. 4.

Chromosome topography: interpretation of the DNA-density map

Further interpretation of the density maps shown in Fig. 4 required that the actual path followed by the polytene chromosomes be traced. This was accomplished by building a wire model using a Richard's optical comparator[37], as is standard in macromolecular X-ray crystallography. Computer-generated half-tone representations transferred to plastic sheets were used instead of density contour maps. Grey-level representations were found to be significantly more interpretable than contour maps. Although only four or five sections could be overlayed at one time, the increased clarity greatly aided the model building. The physical model depicting the chromosomal folding pattern is shown in Fig. 5.

The observed folding pattern is a complex mixture of intertwined coils and parallel chromosome segments, reminiscent of folding patterns seen in proteins. These elements of chromosomal 'secondary structure' are tightly packed against the inner surface of the nuclear membrane. This close membrane association results in a predominantly chromosome-free central cavity. The nucleolus is located in this cavity, but only occupies one-quarter to one-third of the available volume.

At one end of the structure there is an extremely tight cluster of chromosomes, at what is most probably the chromocentre. Several free ends, presumably corresponding to the telomeres, can be seen at the opposite pole. These two loci define a vector that lies perpendicular to the surface of the salivary gland, with the chromocentre positioned towards the surface. In *Drosophila* early embryonic nuclei, the individual centromeres are grouped into a densely staining structure, the chromocentre, during interphase. In *Drosophila virilis* as well as *D. melanogaster* the chromocentre has been rigorously shown to be located near the embryo surface at the cellular blastoderm stage. Barely visible fibres (the chromosomes) trail away towards the centre

Fig. 5 Three views of the wire model constructed using a Richard's box[35] to superimpose the virtual image of the model onto a stack of 'DNA-density' maps mounted on plastic sheets. Note the tight cluster of chromosomes at the chromocentre (C), and the well-defined coiled (H) and parallel regions (P).

of the embryo, again defining a vector normal to the surface (J.W.S., manuscript in preparation). A centromere–telomere polarization has been reported in prophase plant nuclei[20,21]. The observation that such a polarization also exists in both polytene and diploid interphase nuclei suggests that the prophase arrangement is derivative of that seen in interphase. This seemingly fundamental property (polarized chromocentre–telomeres) of interphase and prophase chromosomes may be necessary for the orderly untangling that must accompany condensation and mitosis.

Although the resolution of this reconstruction was quite adequate to determine the overall folding pattern, it was not sufficient to resolve the banding pattern in most regions of the map. As a consequence, it was not possible to identify the individual chromosome arms or to align the genetic map with the topological arrangement. In those instances where a polytene arm ran perpendicular to the image plane, the polytene chromosome was observed in cross-section, revealing that the centre of a band is relatively DNA-free, as suggested by Mortin and Sedat[38].

Preliminary analysis of an adjacent nucleus in the same salivary gland indicates an equivalence at least at the level of gross morphology. This was determined by using a Richard's box to optically superimpose the virtual image of the physical model on the reconstructed density map from the second nucleus. The location and relative arrangement of the major 'secondary structure' features, such as coiled or parallel regions, were found to be similar in the two nuclei, and will be reported in detail elsewhere.

Discussion

As yet, there is no physical model or conceptual framework available for integrating DNA sequence information, structural changes at the nucleosome and higher levels, and genetic data into a coherent picture of how chromosomes function within the cell nucleus. The problem of establishing such a framework is essentially a structural one. It is necessary to understand both the higher-order levels of chromatin organization and how they may be dynamically altered during transcription (as in puffing) as well as to establish the role of the spatial organization of chromosomes within the nucleus during all stages of the cell cycle. The preferential location of specific gene loci at specific sites within the nucleus appears to have important implications for gene control and development[30,31].

A defined spatial arrangement can arise through specific chromosome–chromosome interactions (analogous to protein quaternary structure), through the attachment of specific chromosomal loci to specific sites on the nuclear membrane, or through both. It is quite likely that many of the observed features (such as the tight bends) result from ectopic fibre cross-linking of chromosomal segments. Cytological studies on squashed preparations have identified many specific fibre attachment points[39], although the number determined is probably an underestimate due to preparative damage. The demonstrated inheritance of attachment points indicates that they do not occur randomly and are under genetic control. Sedat and Manuelidis[10] have shown by scanning electron microscope that the polytene chromosomes do not unfold following gentle chemical removal of the nuclear membrane, although they do collapse inwards onto the nucleolus. This suggests that the chromosomal organization is primarily maintained by chromosome–chromosome interactions, and that nuclear–membrane attachement is mainly used to support and orientate the entire assembly. The observation that the chromocentre is always orientated towards the outside of the gland or embryo indicates that the overall orientation is carefully maintained.

The determination of the limits of variability, and the correlation with factors that might influence the spatial organization requires a comprehensive analysis of a large number of nuclei. Techniques for the parameterization and refinement of the current physical model need to be developed and applied to higher resolution reconstructions. It is also necessary to align the genetic map with the observed topological folding pattern in order to correlate genetic effects at specific loci with their spatial location. This work is under way.

The study of many cellular processes such as mitosis, intracellular transport, cytoskeletal organization and rearrangements, compartmentalization and neural organization have all been hampered by the inability to analyse the relevant structures in three dimensions in living or native material. Cellular tomographic techniques (such as described here) when used in conjunction with specific dyes or monoclonal antibodies should fill this gap. The use of intensified video cameras and direct digital data acquisition should allow a three-dimensional data set to be collected either from very weakly fluorescing specimens by integration methods or very rapidly (a few seconds) from brighter samples, enabling the study of dynamic processes in live tissue.

We thank Dr R. M. Stroud for many helpful discussions and for the use of his Syntex AD1 microdensitometer and Data General Eclipse S230 computer. This work was supported by NIH grant GM25101. D.A.A. was supported by a Helen Hay Whitney postdoctoral fellowship.

Received 22 September 1982; accepted 28 January 1983.

1. Sanger, F. *et al. Nature* **265**, 687–695 (1977).
2. Drew, H., Takano, T., Itakura, K. & Dickerson, R. E. *Nature* **286**, 567–573 (1980).
3. Wing, R. *et al. Nature* **287**, 755–758 (1980).
4. McKay, D. B. & Steitz, T. A. *Nature* **290**, 744–749 (1981).
5. Anderson, W. F., Ohlendorf, D. H., Takada, Y. & Matthews, B. W. *Nature* **290**, 754–758 (1981).
6. Finch, J. T. & Klug, A. *Cold Spring Harb. Symp. quant. Biol.* **42**, 1–9 (1977).
7. Klug, A., Rhodes, D., Smith, J., Finch, J. T. & Thomas, J. O. *Nature* **287**, 509–516 (1980).
8. Kornberg, R. D. *A. Rev. Biochem.* **46**, 931–954 (1977).
9. Marsen, M. P. F. & Jaemmli, U. K. *Cell* **17**, 849–858 (1979).
10. Sedat, J. & Manuelidis, L. *Cold Spring Harb. Symp. quant. Biol.* **42**, 331–349 (1977).
11. Bak, A. L., Zeuthen, J. & Crick, F. H. C. *Proc. natn. Acad. Sci. U.S.A.* **74**, 1595–1599 (1977).
12. Paulsen, J. R. in *Electron Microscopy of Proteins* Vol. 3 (ed. R. Harris) Ch. 4 (Academic, London, 1982).
13. Inoué, S. & Sato, H. in *Molecular Architecture in Cell Physiology* (eds Hayashi, T. & Szent-Gyorgy, A.) 209–239 (Prentice-Hall, New Jersey, 1964).
14. Agard, D. A. & Sedat, J. W. *Proc. Soc. Photo-Opt. Instr. Engng* **264**, 110–117 (1980).
15. Agard, D. A. & Sedat, J. W. (in preparation).
16. Wilson, E. B. *The Cell in Development and Heredity* 3rd edn, pp. 215–225 (Macmillan, New York, 1925).
17. Finch, R. A., Smith, J. B. & Bennett, M. D. *J. Cell Sci.* **42**, 391–403 (1981).
18. Miller, O. J., Mukherjee, B. B., Breg, W. R. & Gamble, A. van N. *Cytogenetics* **2**, 1–1 (1963).
19. Lacadena, J. R. & Ferrer, E. *Chromosoma* **67**, 77–86 (1974).
20. Ashley, T. *J. Cell Sci.* **38**, 357–367 (1979).
21. Rabl, C. *Morph. Jb.* **10**, 214–330 (1885).
22. Thomas, H. *Chromosoma* **42**, 87–94 (1973).
23. Avivi, L., Feldman, M. & Bushuk, W. *Genetics* **62**, 745–752 (1969).
24. Sved, J. A. *Genetics* **53**, 747–756 (1966).
25. Davies, H. G., Murray, A. B. & Walmsley, M. E. *J. Cell Sci.* **16**, 261–299 (1974).
26. Murray, A. B. & Davies, H. G. *J. Cell Sci.* **35**, 59–66 (1978).
27. Robinson, S. I., Nelkin, B. D. & Vogelstein, B. *Cell* **28**, 99–106 (1982).
28. Werry, P. A. Th. J., Stoffeben, K., Engles, F. M., van der Jaan, F. & Spanjers, A. W. *Chromosoma* **62**, 93–101 (1977).
29. Evans, H. J. & Bigger, T. R. C. *Genetics* **46**, 277–289 (1961).
30. Jack, J. W. & Judd, B. H. *Proc. natn. Acad. Sci. U.S.A.* **76**, 1368–1372 (1979).
31. Bingham, P. M. *Genetics* **95**, 341–353 (1980).
32. Beerman, W. *Protoplasmatologia* **60**, 1–152 (1962).
33. Castleman, K. R. *Digital Image Processing*, 351–360 (Prentice-Hall, New Jersey, 1979).
34. Weinstein, M. & Castleman, K. R. *Proc. Soc. Photo-Opt. Instr. Engng* **26**, 131–138 (1971).
35. Stokseth, P. A., *J. opt. Soc. Am.* **59**, 1314–1321 (1969).
36. Agard, D. A., Steinberg, R. A. & Stroud, R. M. *Analyt. Biochem.* **111**, 257–268 (1981).
37. Richards, F. M. *J. molec. Biol.* **37**, 225–230 (1969).
38. Mortin, L. & Sedat, J. W. *J. Cell Sci.* **57**, 73–113 (1982).
39. Kauffman, B. P. & Iddles, M. K. *Port. Acta. Biol.* **A7**, 225–248 (1963).